

COUPLING AND DECOUPLING SECONDARY D-Q CURRENTS BASED BRUSHLESS DOUBLY-FED RELUCTANCE MACHINE

Mohammed Saadi Hassan
Lecturer, College of Engineering, University of Diyala
E-mail: msdi981@gmail.com

ABSTRACT: - The paper presents the comprehensive study about the Coupling and decoupling behaviour occurs on Brush-less Doubly Fed Reluctance Machine 'based voltage and flux oriented control which are realized mathematically. The main motivation for studying this project is the relative simple control strategy and optimising Brushless doubly fed performance. The presence of (dSPACE) application is considering the first requirements for real time implementation RTI simplified and proof the different method algorithms to cover the necessary change occurring in deferent speed mod based vector control VC which is considered the one of qualified control application matching with FOC Approach.

Keywords:-Brushless doubly-fed reluctance machine, coupling and decoupling behaviors ,VC&FOC,reference frame and RTI.

1. INTRODUCTION

The risk of depletion conventional energy resources in the near future ⁽¹⁾ was imperative reasons for the researchers in the energy field to track for permanent sources and environmentally friendly such as wind energy .Wind power plants have been added advantage that they widely available worldwide and can't be deserted ^(2,3), due the rising amount of wind turbines worldwide .Brushless Doubly Fed Reluctance Brushless Doubly-Fed Machines (BDFM) have been considered as a potential alternative to the existing solutions in applications with limited variable speed capability (such as wind turbines and large pumps ⁽⁴⁾. The main reasons for this interest by the academic and industrial communities lie in the BDFM attractive features which are in many respects similar to the conventional

DFIG: competitive performance at low cost afforded by the use of a smaller inverter relative to the machine rating. Unlike the DFIG, however, the BDFM has a brushless structure which should bring further advantages in terms of higher reliability and maintenance-free operation with immediate implications on operation and maintenance cost reductions. These can be particularly high in off-shore wind turbine Installations ⁽⁵⁾, where the BDFM use would be highly beneficial from this point of view.

The BDFM comes in two distinct design types: with a special nested cage rotor, known as the brushless doubly-fed induction machine (BDFIM) and with a cage-less reluctance rotor which can be similar (although not the most optimal) as a modern synchronous reluctance machines Figure(1). The latter BDFM form is called the brushless doubly-fed reluctance machine and this will be the focus of research in this project. The rational for considering this type is behind its simpler dynamic modeling, lower machine parameters dependence and easier control compared to its BDFIM counterpart. All these salient features of the BDFRM have been afforded by its 'cold' rotor design and absence of rotor windings ⁽⁶⁾.

As a two stator windings, the primary (power) winding is grid connected and the secondary (control) winding is converter fed, with deferent pole numbers and a salient pole rotor ⁽⁷⁾. The stator windings (p-primary and s-secondary) are magnetically coupled by themselves in harmony with the rotation the reluctance rotor which makes this possible. The presence of the variable reluctance path of disturbance flux in the machine modulates essentially the stator MMF waveforms, corresponding to the flux density harmonics, which can link to the opposite winding. The torque production occurs as a result of electro-mechanical energy conversion response in the machine. In order to avoid coupling in frequency, BDFRM is designed with deferent stator pole numbers of primary and secondary windings. Furthermore, the number of rotor poles should be one-half the total number of stator poles. One of the unique behaviors of BDFRM is that it can operate to perform various functions ^(8, 9). For example it can operate as conventional induction machine by simply shorting the secondary winding even such action protect the control side in the case of inverter failure. Currently, this mode is used to start the machine which was also followed in the laboratory work. A second feature is that when the secondary winding is fed with DC voltage, the machine behaves like synchronous-machine. Finally, when partially coupled with a converter, BDFRM acts in a manner similar to any conventional doubly exited induction machine that is commonly used for wind power conversion and its Vector control based voltage frame or flux oriented control based flux frame which monitor several variables simultaneously, further to the consequences of compliance associated with cost implications. The brushless doubly fed machine operates at specific magnetic-flux level as mentioned in ⁽¹⁰⁾. This level is introduced when the rated voltage is applied at rated frequency. The rotor speed can control by the secondary slip frequency and the machine can easily controlled to run either in super or sub-synchronous speed.

2- DYNAMIC MODEL FOR BDFRM.

Following the dynamic model equations for the BDFRM, permit as to understand the main prospect for the control theory.

$$U_p = R_p i_p + \frac{d\lambda_p}{dt} \Big|_{\theta_p=\text{cont}} + j\omega_p \lambda_s \quad (1)$$

$$U_s = R_s i_s + \frac{d\lambda_s}{dt} \Big|_{\theta_s=\text{cont}} + j(\omega_r - \omega_p) \lambda_p \quad (2)$$

Mathematical relationship between the electrical rotation angle ω_r and mechanical rotation angle ω_{rm} consider the main prospect to coupling relation for BDFRM determined by the equation:

$$\omega_{rm} = \frac{\omega_p + \omega_s}{P_r} \leftrightarrow \omega_r = \omega_{rm} p_r = \omega_p + \omega_s \quad (3)$$

Angular velocity ω_r [rad/sec] defined as the sum of primary and secondary winding frequencies [rad/sec]. Based on equation (3) can built appropriate rotating frame angle θ_r flanked by the primary and secondary location frame angel in the both side machine winding as follows:

$$\begin{cases} \theta_{rm} = \int \omega_{rm} dt \\ \theta_{p,s} = \int \omega_{p,s} dt \end{cases} \quad (4)$$

$$\theta_r = \theta_{rm} p_r = \theta_p + \theta_s \quad (5)$$

$$\begin{cases} \lambda_p = L_p i_p + L_{ps} i_s^* e^{j\theta_r} = \lambda_p e^{j\theta_p} \\ \lambda_s = L_s i_s + L_{ps} i_p^* e^{j\theta_r} = \lambda_s e^{j\theta_s} \end{cases} \quad (6)$$

The subscripts 'p & s' donate primary and secondary quantities respectively (*) present complex conjugate for alternative currents inside the BDFRM winding. The frame flew for the secondary voltage start with the stationary angle θ_p in the primary side shifted as rotating angle θ_r to draw secondary voltage angle θ_s .

The next vector chart will describe the orientation of secondary voltage proportion to primary voltage frame.

There are many possible equations ⁽¹¹⁾ for the electrical torque expression but the most important expression in control application is given in equation (7):

$$T_e = \frac{3P_r L_m}{2L_p} (\lambda_{pd} i_{sq} + \lambda_{pq} i_{sd}) \quad (7)$$

Where, λ_{pd} and λ_{pq} primary winding are fed from constant grid voltage and i_{sd} can be controlled by inverter. When T_e electric torque reacts with mechanical determination counter T_l with a single inertia load (J) ⁽¹³⁾, the output of the equation (8) reflects the derivative of ω_{rm} mechanical angular velocity of the prime mover shaft [rad/sec]:

$$\frac{d\omega_{rm}}{dt} = \frac{1}{J} (T_e - T_l) \quad (8)$$

$$\omega_{rm} = \frac{1}{J} \int (T_e - T_l) dt \quad (9)$$

Preceding of the equation (3) the secondary slip frequency [rad/second] could appear in a different mod as shown in table (1):

$$\omega_s = \omega_{rm} p_r - \omega_p \quad (10)$$

Slip frequency present as command frequency applied to the secondary side. When this command signal is positive, the generated MMFs by the two-stator windings will rotate in the same direction and the machine will increase its speed however negative ω_s means the opposite phase sequence of secondary to primary winding ⁽¹⁴⁾.

The improvement can be satisfied from simple accompaniments voltage and flux with suitable Principle method of the dynamic equation for BDFRM to prove theoretically and mathematically through a review of the properties of the control performance.

3- COUPLING AND DECOUPLING HYPOTHESES BASED VOLTAGE ORIENTED & FLUX ORIENTED CONTROL.

The reference frame relationship between the primary and secondary winding can be estimated depending of primary flux angle technique for FOC algorithm in desecrate form, and the computing the 3-ph primary active (P) and reactive (Q) power ⁽¹⁵⁾. the control method have been responded to the stationary frame voltage ($v_{\alpha,\beta}$) and ($i_{\alpha,\beta}$) obtained from Phase measurements, with control action Bing implemented in the secondary ds-qs frame rotating at ω_s Figure(3).

The conventional expiration for a Y- connected winding with 3-ph sequence applied for calculation:

$$\begin{cases} P = \frac{3}{2} (i_{\alpha} v_{\alpha} + i_{\beta} v_{\beta}) \\ Q = \frac{3}{2} (i_{\alpha} v_{\beta} - i_{\beta} v_{\alpha}) \end{cases} \quad (11)$$

The reactive power is often set to zero ($Q^*=0$) in case unity power factor and (P^*) in open loop speed (i.e. power or torque) mod of the machine .in variable speed WECS, either ω_{rm}^* or (P^*) may correspond to the Maximum Power Point Tracking (MPPT) of wind Turbine ⁽¹⁶⁾.

The essential flux expression for BDFRG space vector mode in primary rotating angle ω_p (e.g. d_p - q_p) ω_s (e.g. d_s - q_s for the secondary winding) ⁽¹⁶⁾.

$$\lambda_p = \underbrace{L_p \cdot i_{pd} + L_m \cdot i_{md}}_{\lambda_{pd}} + \underbrace{L_p \cdot i_{pd} - L_m \cdot L_{mq}}_{\lambda_{pq}} \quad (12)$$

$$\lambda_p = \underbrace{L_s \cdot i_{sd} + L_{md}}_{\lambda_{sd}} + \underbrace{(\delta L_s \cdot i_{sd} + L_{mq})}_{\lambda_{sq}} = \delta L_s i_s + \underbrace{\frac{L_m}{L_p} \lambda_p^*}_{\lambda_m} \quad (13)$$

In the equation (12) the magnetizing current (i_m) and primary flux λ_p in the ω_p frame whereas i_s as a secondary currents and λ_m in equation (13) in $p_r \cdot \omega_{rm} - \omega_p = \omega_s$ frame, as natural frame. The conventional power expression can be presented as:

$$S = P_p + j Q_p = \frac{3}{2} j \omega_p \lambda_p i_p^* \quad (14)$$

By substituting the flux equation (12) and (13) in the (14) the general vector Equation can be developed in term torque and active/reactive power to:

$$T_{evc} = \frac{3}{2} p_r \underbrace{\lambda_{md} i_{sq}}_{T_{foc}} - \frac{3}{2} p_r \lambda_{mq} i_{sd} \quad (15)$$

$$P_{pvc} = \frac{3}{2} \frac{T_{evc}}{p_r} = \frac{3}{2} \underbrace{\omega_p \lambda_{md} i_{sq}}_{P_{pfoc}} - \frac{3}{2} \omega_p \lambda_{mq} i_{sd} \quad (16)$$

$$Q_{pvc} = \frac{3}{2} \omega_p \underbrace{\left(\frac{\lambda_p^2}{L_p} i_{sq} - \lambda_{md} i_{sd} \right)}_{Q_{pfoc}} - \frac{3}{2} \omega_p \lambda_{mq} i_{sq} \quad (17)$$

The complimentary of FOC (e.g. with the d_p -axis aligned with the λ_p as in Figure (2):

$$T_{efoc} = \frac{3}{2} \frac{L_m}{L_p} p_r \lambda_{md} i_{sq} = \frac{3}{2} p_r \lambda_m i_{sq} = \frac{3}{2} p_r \lambda_p i_{pq} \quad (18)$$

$$P_{efoc} = \frac{3}{2} \omega_p \lambda_m i_{sq} = \frac{3}{2} \frac{L_m}{L_p} \omega_p \lambda_p i_{sq} \quad (19)$$

$$Q_{efoc} = \frac{3}{2} \frac{\omega_p \lambda_p}{L_p} (\lambda_p - L_m i_{sd}) = \frac{3}{2} \omega_p \lambda_p i_{pd} \quad (20)$$

Where the λ_{md} , λ_{mq} consider the magnetizing flux component.

The FOC control expression display the power correspondence with the secondary currents in term of using P,Q control strategy in MPPT and satisfying from decoupling advantage over vector control strategy, when the coupling side clear in equation (15,16, 17) as torque and power. The situation is better in FOC when the torque and power are correspondence with one of i_{sd} , and i_{sq} current .Otherwise the if the d_p -axis lies along the λ_p , then the corresponding d_s -axis of the secondary currents aligned with λ_m .such a usual frame-flux vector mapping is inherited with FOC control Strategy Figure (3).

This method of control theories achieved a certain accuracy and sharp response to the sudden changes in the machine speed, when its situated under the influence of non-linear front winds speed ⁽¹⁴⁾. The dynamic model for FOC control more related with primary side than vector control. The design adopted in this investigation satisfied from the speed loop control which involved to this algorithm to create specific torque correlated with reference current i_{sq} (18) as the outcome from first stage controller. Other branch can estimate i_{sd} by comprehensive open loop strategy between the desired and actual reactive power (Q, Q^*) established from the primary side. The cascade control of the theory will decrease the fluctuation in transient period and the PI controller adjusts and limits of the currents and out coming reference voltage V_d, V_q Figure (4).

As can be seen in the above expiration, VC of P_p and Q_p is coupled as both the i_{sd} and i_{sq} secondary current appear in (16) and (17), reducing this coupling can be achieved by aligning q_p -axis of the reference frame to the primary voltage vector as proposed in Fig.6, in this case λ_p would be phase shifted ahead of the corresponding d_p -axis, depending on the winding resistance which is generally smaller in large machine. For this reason the reference frame of the VC should be similar to the FOC control and the equation (19) and (20) can be developed as:

$$P_{vc} \approx P_{efoc} = \frac{3}{2} \omega_p \lambda_m i_{sq} = \frac{3}{2} \frac{L_m}{L_p} \omega_p \lambda_p i_{sq} \quad (21)$$

$$Q_{vc} \approx Q_{efoc} = \frac{3}{2} \frac{\omega_p \lambda_p^2}{L_p} - \frac{3}{2} \omega_p \lambda_{ps} i_{sd} = \frac{3}{2} \frac{\omega_p \lambda_p}{L_p} (\lambda_p - L_{ps} i_{sd}) = \frac{3}{2} \omega_p \lambda_p i_{pd} \quad (22)$$

With the λ_p , λ_{ps} magnitude fixed by primary winding grid connection at line frequency (ω_p) the P_p will be respective to the i_{sq} and Q_p versus i_{sd} as following relation (23)

$$\begin{cases} i_{sq}^* = PI(P^* - P) \\ i_{sd}^* = PI(Q^* - Q) \end{cases} \quad (23)$$

And reference control voltage responded to (24):

$$\begin{cases} v_{sq}^* = PI(I_{sq}^* - I_{sq}) \\ v_{sd}^* = PI(I_{sd}^* - I_{sd}) \end{cases} \quad (24)$$

The inverter has big role to transfer the voltage vectors equation (24) in time vectors to monitor the secondary side machine as a control command.

4- RESULTS IN REAL TIME IMPLEMENTATION

The machine which is implementing in the work 1,5 KW BDFRG Table (2) (Generating Mode) associated Unite DS1103 Controller shown In Figure (5) as a part of BDFRG test rigs. The first step consists in modeling the control system with Simulink and configuring the I/O connections of the Connector Panel thanks to the RTI toolbox. Using RTI automatically generates the C-code for the board. The dSPACE hardware can perform a real-time experiment which can be controlled from a PC with Control Desk Figure (6). Control Desk can be used to monitor the simulation progress, adjust parameters online, capture data (in a format compatible with Matlab) and communicate easily with the computer real-time.

Figure (7) illustrate the RT results which gained respectively under speed trajectory (Super and sub speed) due to $\omega_s \neq 0$ climbing to the velocity 900 rpm or descending to speed 600 rpm which is value and polarity are followed slip frequency ω_s as illustrated in table (1). The analyzing secondary currents and torque behaviors through these deferent trends is our target.

Under generating mode the load torque is varying in negative domain reflecting the nature of extracting torque from the external sources (turbine). The short view for the extracting results as a RTI declared the consequence of coupling on the I_{sd-q} currents and torque (left side) the sequence of change in I_{sq} upshot the I_{sd} obviously ,and that's mean the both currents has equivalent role to describe the shape of torque (old procedure).

The decoupling (right side result) compiles with secondary current to track the dramatic variation in speed mode separately. In order to reach positive results the value of the secondary current $I_s = I_{sq}$, $I_{sd} = 0$) to gain maximum magnetizing currents from the primary side and that's reflected the sole of the MTPAI hypotheses which resolve the lack of magnetizing flux from the primary to secondary side of machine by extracting maximum magnetizing currents from primary stator side presented in I_{sq} current (new procedure)

The current I_{sd} not more responding to I_{sq} variation and the torque track only the reactive current I_{sq} or magnetizing current from primary side machine, so that validate the sudden increasing in reactive power in decoupling case.

5- CONCLUSION.

The main contribution of the work is the comparative development and performance analysis of field (primary flux) oriented control (FOC) and vector (primary voltage oriented) control (VC) algorithms for optimum operation of the BDFRG—a viable, low cost, and reliable alternative to its widely used companion, the conventional slip-ring doubly fed induction generator (DFIG). Such a control framework can serve as a basis for further research on this emerging brushless machine topology for applications with limited variable speed ranges foremost wind turbines (but also large pump-alike drives) where the cost advantages of partially rated power electronics can be fully exploited. The results presented have illustrated the high potential and effectiveness of the control methods considered using the MTPAI strategy which offers the machine efficiency improvement.

REFERENCES

- 1) S. White, "Germany scraps nucleare power after Fukushima disaster," in *Daily Mirror*, 2011.
- 2) E. Muljadi, C. P. Butterfield, J. Chacon, and H. Romanowitz, "Power quality aspects in a wind power plant," in *Power Engineering Society General Meeting, 2006. IEEE*, 2006, p. 8 pp.
- 3) S. White, "Germany scraps nucleare power after Fukushima disaster," in *Daily Mirror*, 2011.
- 4) Z. Ying and L. Hongyan, "Evaluation on comprehensive benefit of wind power generation and utilization of wind energy," in *Software Engineering and Service Science (ICSESS), 2012 IEEE 3rd International Conference on*, pp. 635-638.
- 5) M. G. Jovanovic, R. E. Betz, and Y. Jian, "The use of doubly fed reluctance machines for large pumps and wind turbines," in *Industry Applications Conference, 2001. Thirty-Sixth IAS Annual Meeting. Conference Record of the 2001 IEEE*, 2001, pp. 2318-2325 vol.4.

- 6) M. Jovanovic and R. E. Betz, "Optimal performance of brushless doubly fed reluctance machines," in *Electrical Machines and Drives, 1999. Ninth International Conference on (Conf. Publ. No. 468)*, 1999, pp. 386-390.
- 7) R. E. Betz and M. G. Jovanovic, "Theoretical analysis of control properties for the brushless doubly fed reluctance machine," *Energy Conversion, IEEE Transactions on*, vol. 17, pp. 332-339, 2002.
- 8) L. Ji and X. Yang, "Optimization design on salient pole rotor of BDFRM using the Taguchi method," in *Power Electronics Systems and Applications (PESA), 2011 4th International Conference on*, pp. 1-4.
- 9) M. G. Jovanovic, R. E. Betz, Y. Jian, and E. Levi, "Aspects of vector and scalar control of brushless doubly fed reluctance machines," in *Power Electronics and Drive Systems, 2001. Proceedings., 2001 4th IEEE International Conference on*, 2001, pp. 461-467 vol.2.
- 10) Z. Qian and L. Huijuan, "Comparative Study of Brushless Doubly Fed Machine with Different Rotor Structures Used in Wind Power Generation System," in *Power and Energy Engineering Conference (APPEEC), 2010 Asia-Pacific*, pp. 1-4.
- 11) R. Ancuti, I. Boldea, and G. D. Andreescu, "Sensorless V/f control of high-speed surface permanent magnet synchronous motor drives with two novel stabilising loops for fast dynamics and robustness," *Electric Power Applications, IET*, vol. 4, pp. 149-157.
- 12) R. E. B. M.G.JOVANOVIC, "Introduction to space vector Modeling of the Brushless Doubly fed Reluctance machine," p. 25, 2003.
- 13) H. Chaal and M. Jovanovic, "Flux observer algorithms for direct torque control of Brushless Doubly-Fed Reluctance machines," in *Industrial Electronics, 2009. IECON '09. 35th Annual Conference of IEEE*, 2009, pp. 4440-4445.
- 14) M. G. Jovanovic, J. Yu, and E. Levi, "A review of control methods for brushless doubly-fed reluctance machines," in *Power Electronics, Machines and Drives, 2002. International Conference on (Conf. Publ. No. 487)*, 2002, pp. 528-533.
- 15) Rongfeng, C. Wei, Y. Yong, and X. Dianguo, "Stability improvement of V/F controlled induction motor driver systems based on reactive current compensation," in *Electrical Machines and Systems, 2008. ICEMS 2008. International Conference on*, 2008, pp. 88-90.
- 16) R. E. Betz and M. G. Jovanovic, "The brushless doubly fed reluctance machine and the synchronous reluctance machine-a comparison," *Industry Applications, IEEE Transactions on*, vol. 36, pp. 1103-1110, 2000.

Table (1): Speed modes for BDFRM

| Secondary Slip frequency | Mod Operation | Speed Mode |
|--------------------------|-------------------|-------------------------------------|
| $\omega_s=0$ | Synchronou s-Mode | Synchronous speed =750 [rpm] |
| $\omega_s>0$ | Super Synch-Mode | Super-Sync-Speed >750 to 1000 [rpm] |
| $\omega_s<0$ | Sub sync-mode | Sub-Sync-Speed < 750 to 500 [rpm] |

Table (2): Off-line testing parameters at normal temperature of the 1.5 KW BDFRM prototypes.

| Labels | Parameters | Definition |
|--------------|------------|---|
| f_p | 50 | Grid Frequency [Hz] |
| V_p | 380 | Primary voltage (rms) [V] |
| P_r | 4 | Rotor Poles |
| J | 0.1 | Rotor inertia [kgm^2] |
| R_p | 11.1 | Primary winding resistance [Ω] |
| R_s | 13.5 | Secondary winding resistance [Ω] |
| L_p | 0.41 | Primary winding inductance [H] |
| L_s | 0.57 | Secondary winding inductance [H] |
| $L_{ps}=L_m$ | 0.32 | Mutual inductance [H] |

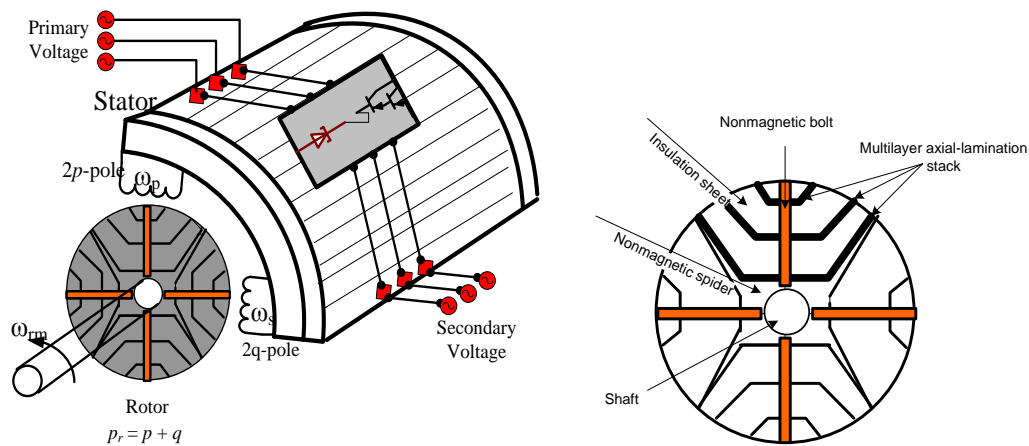


Fig. (1): BDFRM construction (left) Reluctance rotor (right)

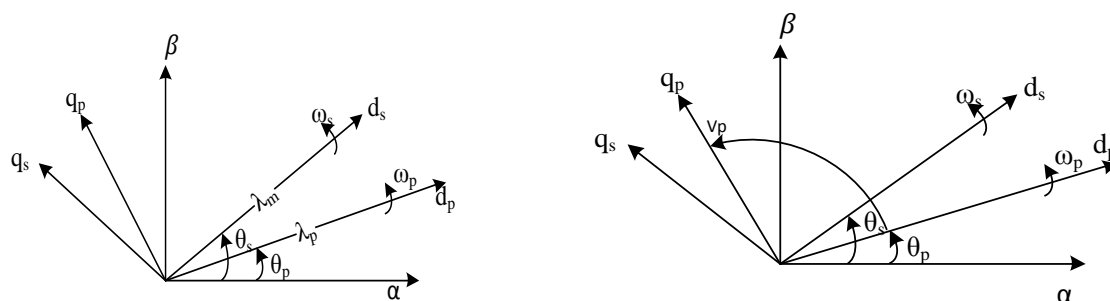


Fig. (2): Reference Frame VC left side FOC right side

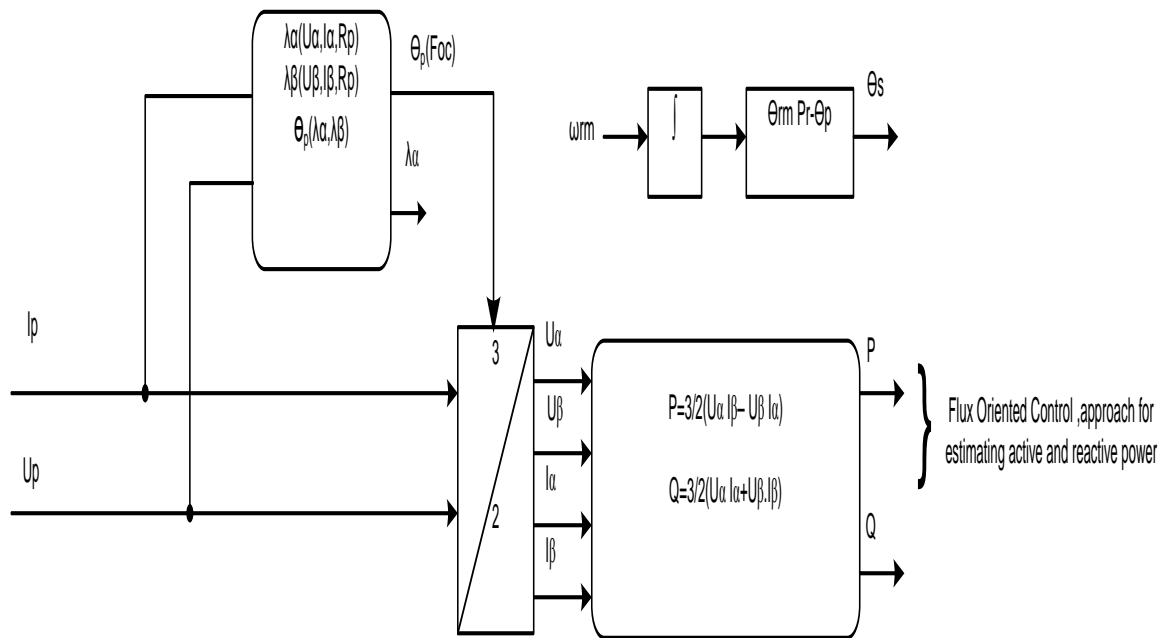


Fig. (3): Reference Frame VC left side FOC right side

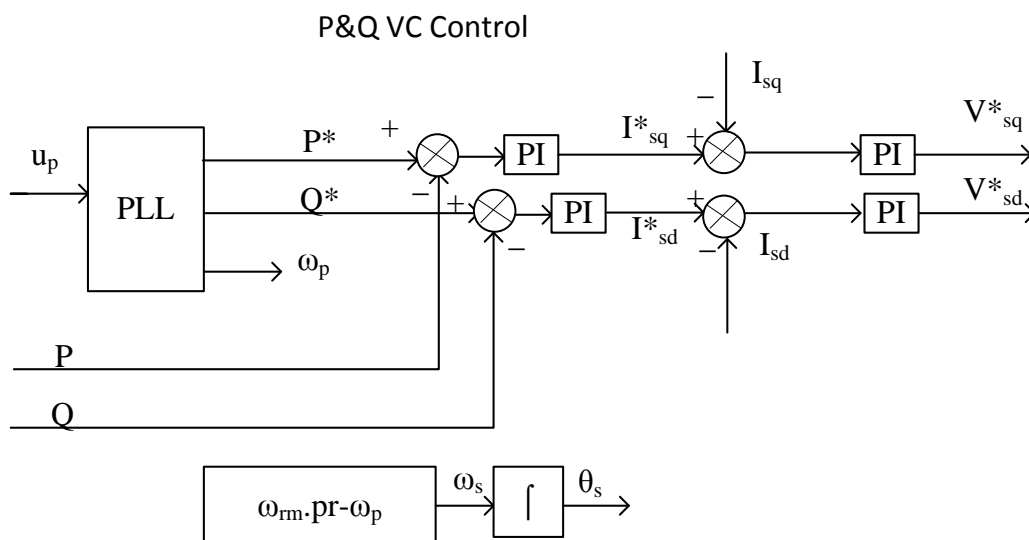


Fig. (4): VC strategy satisfying from FOC approach



Fig. (5): The Lab test rigs for Practice (Actual) evolution

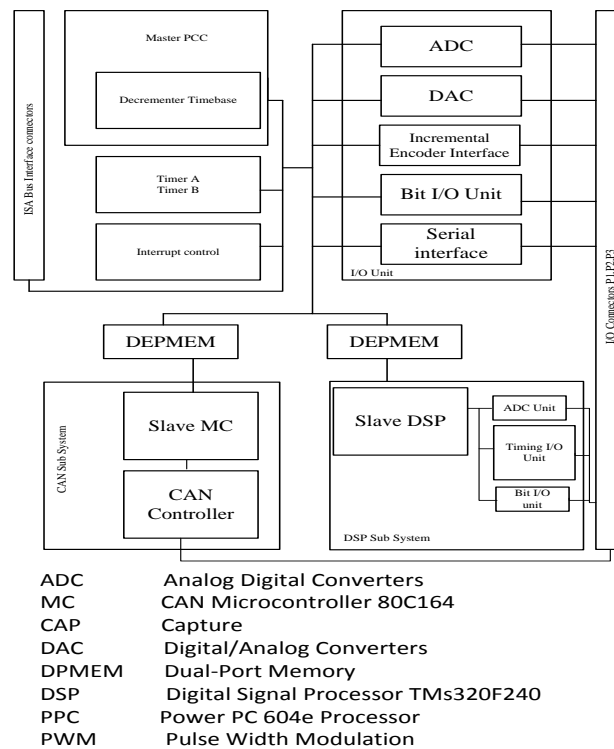


Fig. (6): Block diagram of D-1103 dSPACE

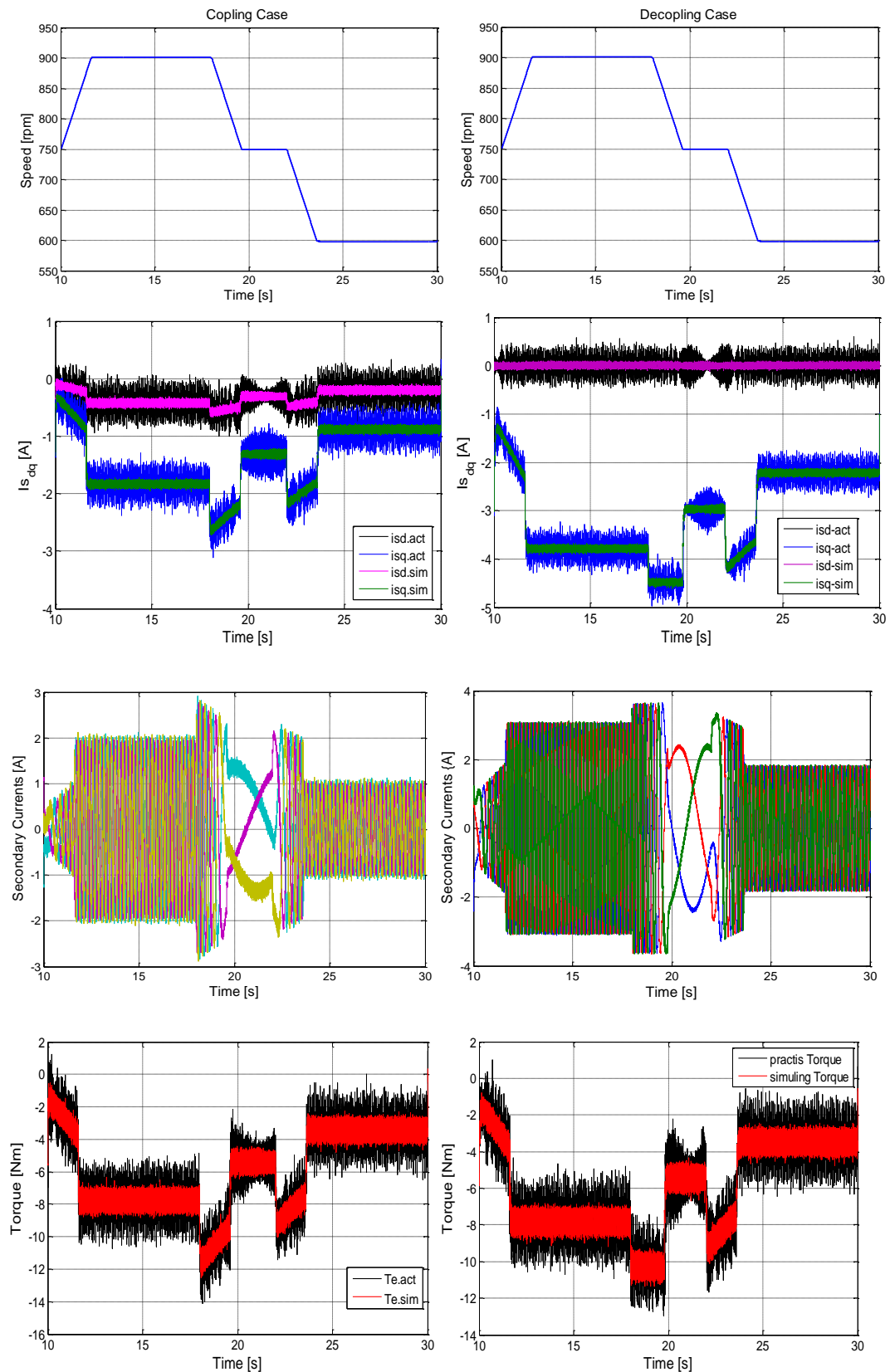


Fig. (7): Secondary d-q currents (upper), Torque and 3PH currents under coupling (left) consequence & decoupling (right).

وصف سلوك الاقتران وعدم الاقتران بين التيارات الثانوية للماكنة ثنائية التغذية

الدكتور محمد سعدي حسن
قسم القدرة والمكائن الكلية الهندسة جامعة ديالى

الخلاصة

تقدم هذه الورقة دراسة تحليلية حول سلوك الاقتران بين التيارات الثانوية في ملفات المولد ثنائي التغذية عديم الفرش اعتمادا على تطبيق التحكم الاتجاهي للفولتية والفيض المغناطيسي التي حققت رياضيا. الدافع الرئيسي لدراسة هذا المشروع هو تبسيط استراتيجية التحكم الاتجاهي ولتحسين أداء المولد . وجود تطبيق (دي سبيس) تعزز من واقعية النتائج المستخلصة في الوقت الحقيقي للتنفيذ RTI التي طورت لتبسيط وإثبات جدارت خوارزميات مختلفة للتحكم. ولتغطية التغييرات اللازمة التي تحدث في مختلف التيارات استنادا الى طريقة التحكم الاتجاهي للفولتية VC والفيض المغناطيسي FOC.